Characterization and modeling of ductile rupture with relationship to microstructures in 2198 Al-Li alloy for aeronautic application

Jianqiang Chen, Jacques Besson, Yazid Madi

Characterization and modeling of ductile rupture with relationship of microstructures in 2198 Al-Li alloy for aeronautic application

Jianqiang CHEN[1*], Jacques BESSON[1], Yazid MADI[1,2]

[1] *Centre des Materiaux, Mines Paristech, CNRS UMR7633, Evry, France;*
[2] *Ermess, EPF – Ecole d'Ingenieurs, Sceaux, France*

Abstract

Damage and fracture mechanisms of two 2198 Al-Li thin sheet alloys having different thicknesses (2 and 6 mm) are investigated. Two heat treatments are studied: T3 and T8. Mechanical tests are carried out on flat specimens including smooth tensile samples and U-notched specimens (with various notch radii). Test data are used to identify the parameters of constitutive equations describing plastic anisotropy. Crack initiation and stable propagation is studied using Kahn tear tests. The microscopic fracture surface of the different specimens is observed using SEM (Scanning Electron Microscopy). Smooth and notched samples exhibit a slant fracture surface. With increasing notch severity, the fracture mode changes significantly. Failure initiates at the notch root in a small triangular region, outside this zone, slant fracture is observed. Observations show two different failure mechanisms with respect to triangular and slant zones.

Key words: 2198 aluminum alloy, ductile rupture, damage growth, crack initiation, crack propagation, fracture mechanisms

1 Introduction

Increasing payload and fuel efficiency of aircrafts has become a major issue for the aerospace industry and led to the development of materials with high specific. The family of lithium containing Al alloys has received much attention for military, space and commercial application because they offer low density, improved specific strength and high stiffness to weight ratio as compared to the commercial 2xxx and 7xxx series aluminum alloys and carbon fiber-reinforced composites, [1].

The marriage of Li to Al offers the promise of substantially reducing the weight of aeronautic alloys, since each 1 wt. % Li added to Al reduces density by 3% and increases elastic module by about 6%. Among these series, 2198 Al-Li alloy, show a good combination of static tensile properties, damage tolerance and formability. For this reason, they have been used for fuselage skin. Aircrafts designers estimate the fracture resistance of fuselage thin sheet using ductile crack growth resistance tests (R-curve tests) carried out on very large center-cracked tension panel M(T), [2]. These large scale tests are expensive and require a large amount of time and material.

* Corresponding author. Tel .: +33 1 60 76 30 49, fax. : +33 1 60 76 30 50
E-mail address: jianqiang.chen@mines-paristech.fr (J.Chen).

However, they could possibly be replaced by tests on small size Kahn specimens, [3], which also allow for stable crack propagation. The aim of this project is to develop a methodology to predict results on large specimens from results on small ones. The main difficulty is that Kahn samples are under large scale yielding whereas M(T) specimens are designed to be under small scale yielding.

This paper deals with mechanical testing, metallographic observation and failure mechanisms of two 2198 thin sheets having different thicknesses: 2 and 6 mm. Two heat treatments (T3 and T8) where applied to these sheets. Mechanical tests are carried out on flat specimens including smooth tensile samples and U-notched samples with various notch radii. Test data are used to identify the parameters of constitutive equations describing plastic anisotropy. Crack initiation and stable propagation is studied using Kahn tear tests. Macroscopic and microscopic fracture surfaces of the different specimens are observed and the rupture mechanisms are analyzed.

2 Test materials

2198 is a derivate of the alloy 2098, which was developed by McCook Metals to respond to high load on some fuselage parts of the F-16 fighter Aircraft, [4]. 2198 was developed by Alcan CRV, which has slightly lower copper content compared to 2098 and has some other minor chemistry adaptations, to optimize toughness. Table 1 gives the chemical compositions limits of 2198 alloy. In this paper, two grades of 2198 aluminum-lithium alloy sheets with a nominal thickness of 2 mm and 6 mm are supplied by Alcan Centre de Recherches de Voreppe (CRV). They are referred respectively to as R (recrystallized) and F (fibred). For each sheet, two different heat treatments (T3 and T8) were applied. Table 2 gives the nomenclature of the various materials.

Table 1 Chemical compositions limits of 2198 alloy (weight percent).

Si	Fe	Cu	Mn	Mg	Cr	Zn	Zr	Li	Ag
≤ 0.08	≤ 0.1	2.9–3.5	≤ 0.5	0.25–0.8	≤ 0.05	≤ 0.35	0.04–0.18	0.8–1.1	0.10–0.5

Table 2 Tested sheets (2198)

Grain Structure \ Heat treatment	T3	T8
Recrystallized	T3R_2	T8R_2
Fibred	T3F_6	T8F_6

The four sheets have similar chemical compositions. All sheets were solution treated, quenched and naturally aged to a substantially stable condition (T3 heat treatment: T3R_2 and T3F_6). Then an artificial ageing step was preformed to obtain T8 heat treatment (T8R_2 and T8F_6). In the following, the rolling direction is referred to as

L, the long transverse direction as T and the short transverse direction (thickness) as S. D stands for the diagonal direction (45^o between direction L and T in the sheet). The optical micrographs of the grain structure after etching with Keller's etch are shown in Figure 1.

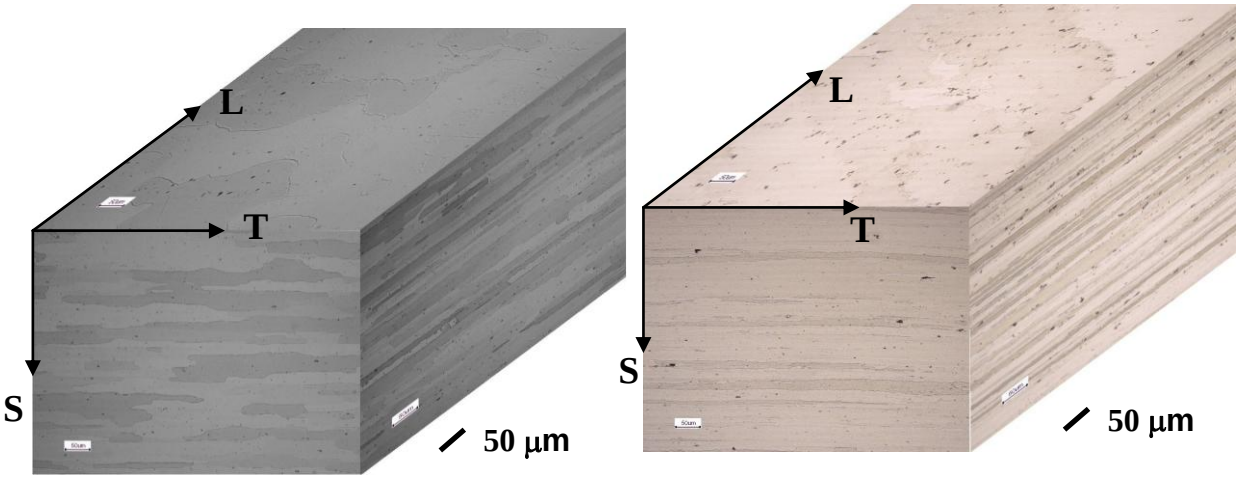

Figure 1 Pseudo three-dimensional microstructure of 2198 T3R_2 (left) and T3F_6 (right) materials (optical microscopy). Polarized light micrographs of the chemical erosion microstructure reveal the grains of the material.

3 Mechanical testing

In order to characterize the alloys' mechanical behavior, four specimens types are used (Figure 2). The TR sample is a conventional smooth tensile bar used to determine the elastic-plastic behavior. The differently notched samples EU1 and EU2 are used to characterize the fracture behavior under various stress triaxiality ratios. Kahn specimens which allow stable crack propagation over more than 20 mm are used to characterize crack initiation and growth, [3].

3.1 Experimental setup and testing conditions

All tests are carried out at room temperature on a servo-hydraulic testing machine under displacement control. The specimen thickness is that of the as-received materials. Tests conducted on smooth specimens are performed along three different directions (L, T and D); U-notched and Kahn specimens are tested in two directions (L and T). Three specimens at least are tested in each condition. Scatter is negligible so that only one curve is plotted in the following.

Kahn specimens are not pre-cracked. The test consists of stretching the specimen with two pins. A 50 kN load cell is used and the cross head speed is 0.1 mm/min. Applied force F and crack tip mouth opening displacement (CMOD) are measured. Straight lines parallel to the loading direction are drawn each millimeter from the notch root to enable crack length measure on pictures taken with a fixed digital camera. With this method, the measured crack length is relative to the initial geometry.

For notched specimens EU1 and EU2, opening displacements were measured on both sides and the mean value was used. Smooth tensile specimens TR were used with two displacements gages so that both longitudinal and transverse strains were recorded. A 50 kN cell was used and the cross head speed was 0.2 mm/min for all cases. Tests conducted at different strain rates (10^{-4} – 10^{-1} s^{-1}) show that strain rate only slightly affects the plastic behavior of these materials.

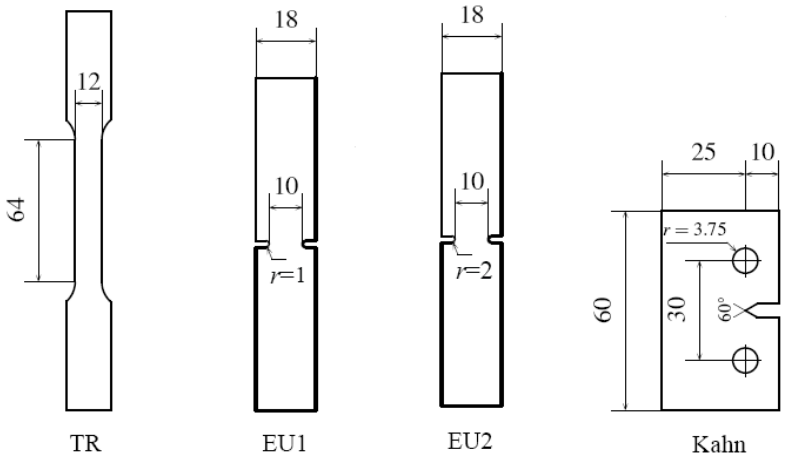

Figure 2 Specimens for mechanical tests (all dimensions in mm) – For TR tensile specimens, longitudinal and transverse deformations are measured. For EU1 and EU2 notched specimens, left and right opening displacements are measured. For Kahn the crack opening displacement and the crack length are measured. The notch radius of Kahn is less than 60 μm.

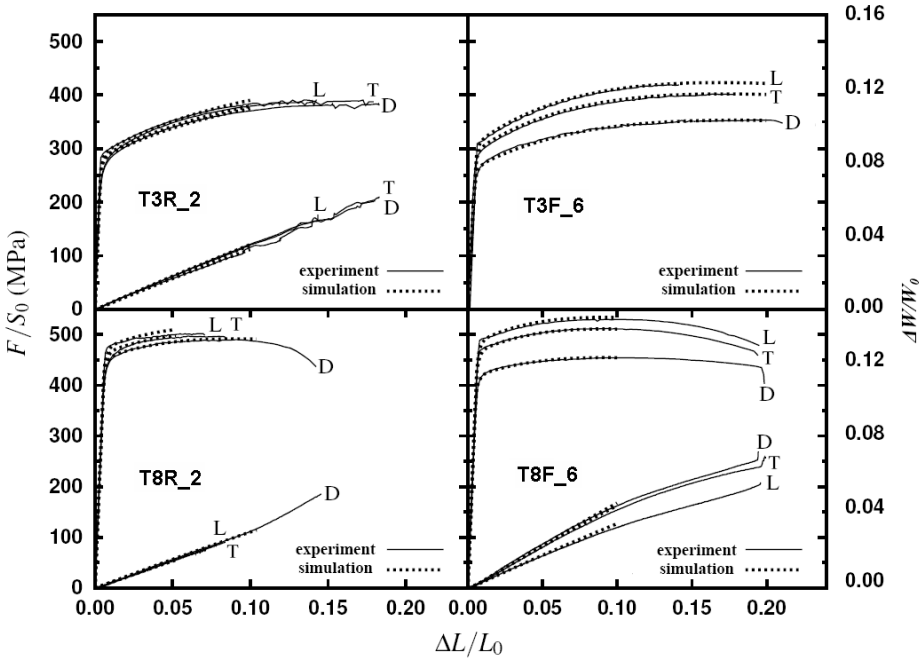

Figure 3 Experiments on smooth specimens in three directions for 2198 material. *F* stands for the load and S_0 for the initial cross section. $\Delta L/L_0$ is the longitudinal elongation. $\Delta W/W_0$ *is* the transverse strain.

3.2 Results

Figure 3 shows the results of tests performed in the L, T and D directions for smooth specimens. As expected T8 treatment hardens both materials. The recrystallized material for both heat treatments exhibits an almost isotropic plastic flow behavior. For all three testing directions deformations in the transverse direction $\Delta W/W_0$ are similar but differ from what would be obtained for an isotropic material. This indicates that the material is transversally isotropic. In the case of the fibred material plastic flow anisotropy is strong with D being the weakest direction and L the strongest as already reported for Al-Li alloys, [6].

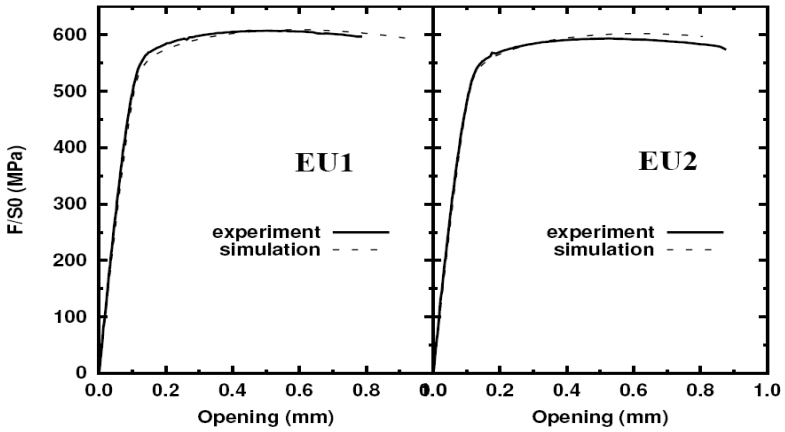

Figure 4 Experiments and simulation results on notched specimens in T direction for 2198 T8F_6. *F* stands for the load and S_0 for the initial cross section.

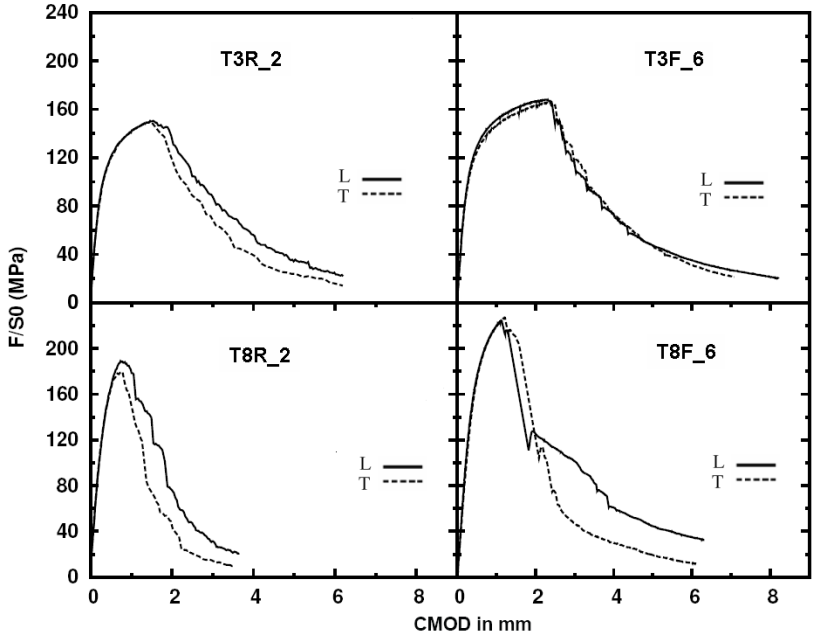

Figure 5 Experiments on Kahn specimens in two directions (L and T) for 2198 materials. *F* stands for the load and S_0 for the initial ligament section

Figure 4 shows results for U-notched specimens with notch radii of 1 mm and 2 mm in the case of the T8F_6 material along the T direction. The maximum stresses obtained along the L and T directions are identical.
Figure 5 displays the load–opening curves for Kahn samples. The toughness difference between each material is significant: T3 sheets have a higher toughness than T8 sheets, but the limit load of T8 sheets is higher than that of T3 sheets; it is higher for fibred sheets (6mm) than for recrystallized sheets (2mm). It is consistent with ultimate tensile strength (UTS) obtained on tensile tests (Figure 3). In all cases crack growth starts when the limit load is reached. Subsequent load drop is due to crack advance. It is faster for the recrystallized material for both heat treatments for specimens loaded along the T direction (cracks propagating along the L direction). Note that plane plastic anisotropy is negligible for this material which consequently exhibits a clear anisotropic fracture behavior. It is almost isotropic for fibred materials. The slight load increase observed for material T8F_6 after initial crack advance is due to crack bifurcation.

4 Fractography

The appearance of the fracture surface depends on the notch severity. Kahn specimens exhibit the following aspect: the crack begins with a flat triangular shape perpendicular to the loading direction. The triangle has its base on the notch root and its maximum height is about half of the sheet thickness. Following this region, a slant fracture surface emerges. This is consistent with the evolution of the triaxial stress and strain state. In the triangular region high stress triaxiality is encountered during crack initiation, while a lower stress triaxiality associated with a plane strain state along the crack propagation direction is encountered in the slanted region [5]. This state is consistent with the formation of an inclined localization band [8]. Figure 6 shows the fracture surface of a broken Kahn sample. For EU1, EU2 and smooth specimens, there is no triangle and the whole surface is slanted.

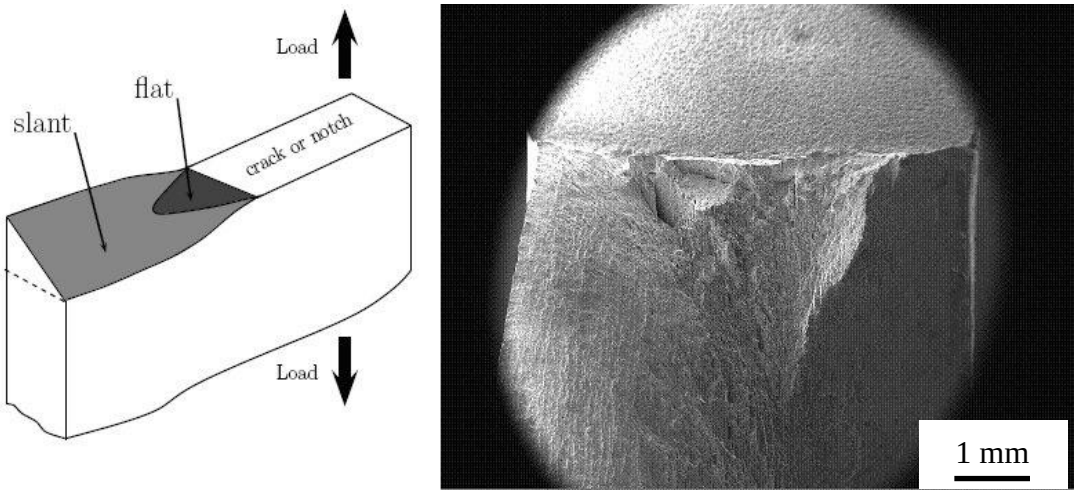

Figure 6 Schematic view of the Kahn fracture surface (left) and observation of a actual Kahn fracture surface for T8F_6 sheet (right).

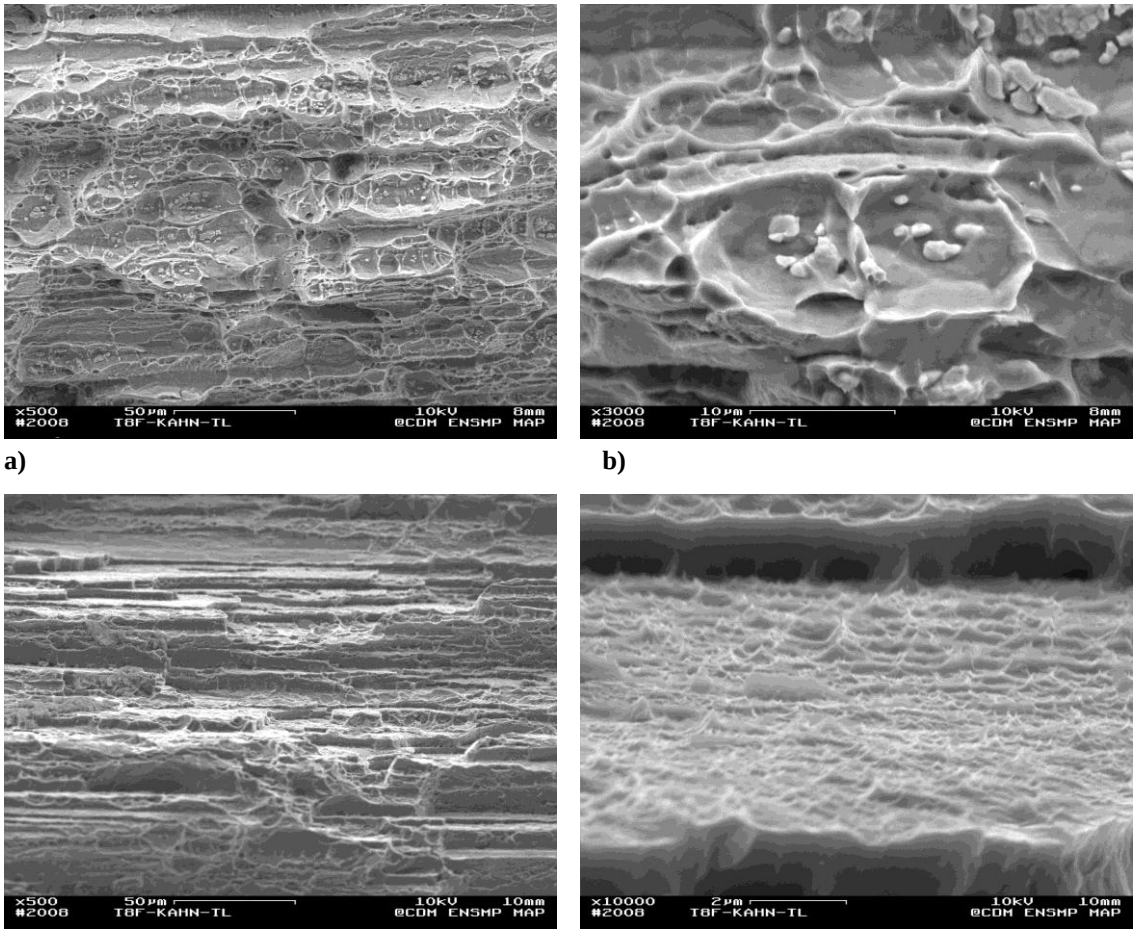

a) **b)**

c) **d)**

Figure 7 Large dimples in triangular zone (a) and (b), micro-dimples in slanted zone (c) and (d) in Kahn sample for 2198 T8F_6 sheet

For Kahn samples, in triangular zone (Figure 7 a) and b)) void growth mechanism is dominant: large dimples can be seen around second phase particles. Their size is about 10 µm. On the contrary, in the slanted zone (Figure 7 c) and d)) void growth is limited and very small secondary dimples are observed. Their size is less than 1 µm.

Standard strain localization analysis, [8], indicates that under plane strain conditions, the fracture surface is normally slanted with a 45 degrees angle with respect to the loading direction. In this study, for T3R_2 and T8R_2 materials, the slant surface is with about 45 degrees with loading direction. However, for the fibred sheets (T3F_6 and T8F_6), the fracture surface angle varies according to the location as showed on Figure 8 so that a steeper fracture plane is obtained.

Figure 8 (left) gives the cross section of a broken Kahn sample (T8F_6 sheet); the angle is about 30 degrees at the center and is near to 45 degrees at the edges. To better understand these phenomena, an observation of the cross section is realized; first a nickel coating was deposited to protect the fracture surface. The cross section was then polished. The optical micrographs of the grain structure after etching are shown

on Figure 8 (right). On the grain boundary, broken particles and holes can be seen. Decohesion at grain boundaries is observed. As grains are strongly elongated along the L and T directions (see Figure 1), a steeper fracture angle could possibly be obtained due to grain decohesion. The failure mode is possibly caused by the development of a tensile stress along the thickness direction (S) due to necking ahead of the crack. These stresses are indeed smaller for a 2mm thick sheet: this could account for the fact that the recrystallized material exhibits a standard slanted fracture plane.

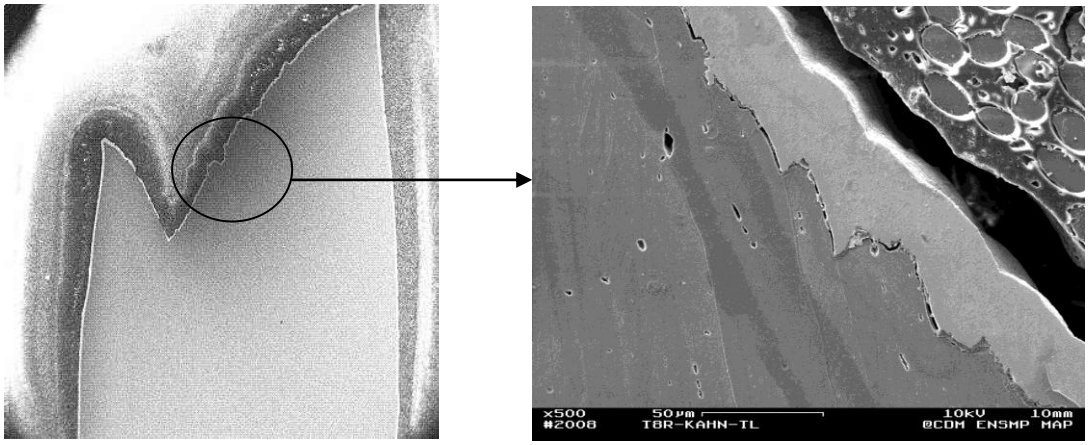

Figure 8 Cross section of broken Kahn fracture sample for 2198 T8F_6 sheet

5 Modeling of anisotropic plastic behavior.

In this section, a model is proposed to represent the plastic anisotropy observed on the materials. Correctly describing plastic anisotropy is important to obtain a realistic description of local strains and stresses needed to assess fracture mechanisms. The yield function proposed in [7] for sheet materials is used in this study. The yield surface is assumed to expand isotropically (isotropic hardening) and is expressed as: $\varphi = \bar{\sigma} - R(p) = 0$ where $\bar{\sigma}$ is an anisotropic stress measure defined as:

$$\bar{\sigma} = \left(\alpha \left(\psi^1\right)^{a/b^1} + (1-\alpha)\left(\psi^2\right)^{a/b^2} \right)^{1/a} \qquad (1)$$

with

$$\psi^1 = \frac{1}{2}\left(|S^1_2 - S^1_3|^{b^1} + |S^1_3 - S^1_1|^{b^1} + |S^1_1 - S^1_2|^{b^1} \right) \qquad (2)$$

$$\psi^2 = \frac{3^{b^2}}{2^{b^2}+2}\left(|S^2_1|^{b^2} + |S^2_2|^{b^2} + |S^2_3|^{b^2} \right) \qquad (3)$$

where $S^k_{i=1-3}$ are the principal values of a modified stress deviator $\underline{s}^k$ defined as follows:

$$\underline{s}^k = \underline{\underline{L}}^k : \underline{\sigma} \qquad (4)$$

with

$$\underline{\underline{L}}^k = \begin{bmatrix} \left(c_2^k + c_3^k\right)/3 & -c_3^k/3 & -c_2^k/3 & 0 & 0 & 0 \\ -c_3^k/3 & \left(c_3^k + c_1^k\right)/3 & -c_1^k/3 & 0 & 0 & 0 \\ -c_2^k/3 & -c_1^k/3 & \left(c_1^k + c_2^k\right)/3 & 0 & 0 & 0 \\ 0 & 0 & 0 & c_4^k & 0 & 0 \\ 0 & 0 & 0 & 0 & c_5^k & 0 \\ 0 & 0 & 0 & 0 & 0 & c_6^k \end{bmatrix} \qquad (5)$$

R (p) corresponds to the flow stress expressed as a function of the cumulated plastic strain *p*. *R (p)* is expressed:

$$R\,(p) = R_0\left[1 + K_0 p + K_1\left(1 - e^{-k_1 p}\right) + K_2\left(1 - e^{-k_2 p}\right)\right] \qquad (6)$$

Identification of the various model parameters is carried out using test results on TR12, EU1 and EU2 specimens. Table 3 gives all model parameters used for the three materials. Simulation and experiments are compared on Figure 3 and Figure 4.

Table 3 Model parameters

a) Elastic – plastic behavior

	E (GPa)	ν	R_0 (MPa)	K_0	K_1	k_1	K_2	k_2
T8F_6	74	0.3	450	0	0.093	655	0.292	16.5
T3R_2	74	0.3	290	3.543	0.087	643	0.293	16.7
T8R_2	74	0.3	450	0	0.091	641	0.277	15.9

b) Anisotropy (c_1^5, c_1^6, c_2^5 and c_2^6 cannot be determined and are set to 1)

	a	α	c_1^1 / c_2^1	c_1^2 / c_2^2	c_1^3 / c_2^3	c_1^4 / c_2^4	c_1^5 / c_2^5	c_1^6 / c_2^6
T8F_6	16.9	0.700	1.152	1.132	0.604	1.183	1	1
			0.647	0.756	1.432	1.213	1	1
T3R_2	16.1	0.680	1.247	1.274	0.799	1.003	1	1
			0.700	0.766	1.537	1.297	1	1
T8R_2	13.7	0.700	1.158	1.192	0.856	1.061	1	1
			0.731	0.793	1.366	1.113	1	1

6 Concluding remarks

In this study four 2198 Al-Li alloy sheets which have different heat treatments and thicknesses were investigated. Due to processing all sheets present an anisotropic plastic behavior both in terms for flow stress and deformation. This behavior is well reproduced by the model developed in [7].

Smooth and notched samples exhibit a slant fracture surface. With increasing notch severity (Kahn tear test), the fracture mode changes significantly. Failure initiates at the notch root in a small triangular region, outside this zone, slant fracture is observed. Observations show two different failure mechanisms with respect to triangular and slant zones. In the triangular zone, under a high hydrostatic pressure, void growth leads to large dimples. On the contrary, in the slanted zone, low hydrostatic pressure together with a plane strain state leads to the localization of the deformation into an inclined band and the nucleation of smaller dimples.

Acknowledgements

This work is part of a global study the third generation Al-Li alloy, research partnership between ALCAN CRV, EADS IW, ENSMP, ENSMA and INPG. We thank all the members of our cooperation.

References

[1] T.S.Srivatsan, E.J.Lavernia, The effect of oxides on mechanical properties of aluminium-lithium alloy. J.Mater.Sci. 888-891, 1990
[2] ASTM, E561-98 Standard practice for R-curve determination, Annual Book of ASTM Standards 03.01,1998
[3] ASTM, B871-01 Standard test method for tear testing of aluminum alloy products, Annual Book of ASTM Standards, 2001
[4] M.Knüwer, J.Schumacher, H.Ribes, F.Eberl and B.Bes. 2198–Advanced Aluminium-Lithium alloy for A350Skin sheet application P.9, 2006
[5] F.Bron, J.Besson, A.Pineau, Ductile rupture in thin sheets of two grades of 2024 aluminum alloy, 2002
[6] D.Steglich, H.Wafai,W.Brocks, Process, Mechanical and heat Treatment Modeling:Anisotropic Deformation and Damage in Aluminum 2198 T8 Sheets. 1239-1240, 2008
[7] F.Bron, J.Besson, A yield function for anisotropic materials application to aluminium alloys, 2004
[8] A.Needleman, J.R.Rice, Limits to ductility set by plastic flow localization. In: Koistinen, D.P,Wang, N.-M.(Eds.), Mechanics of sheet metal forming: material behavior and deformation analysis. Plenum Press, pp. 237-267, 1978